Journal of the Korean Nuclear Society
Volume 29, Number 1, pp. 45~57, February 1997

An Experimental Investigation of Direct Condensation of Steam Jet in Subcooled Water

Yeon Sik Kim, Moon Ki Chung, and Jee Won Park
Korea Atomic Energy Research Institute
150 Dukjin-dong, Yusong-gu, Taejon 305-353, Korea

Moon-Hyun Chun
Korea Advanced Institute of Science and Technology
Department of Nuclear Engineering
373-1 Kusong-dong, Yusong-gu, Taejon 305-701, Korea

(Received May 11, 1996)

Abstract

The direct contact condensation phenomenon, which occurs when steam is injected into the subcooled water, has been experimentally investigated. Two plume shapes in the stable condensation regime are found to be conical and ellipsoidal shapes depending on the steam mass flux and the liquid subcooling. Divergent plumes, however, are found when the subcooling is relatively small. The measured expansion ratio of the maximum plume diameter to the injector inner diameter ranges from 1.0 to 2.3. By means of fitting a large amount of measured data, an empirical correlation is obtained to predict the steam plume length as a function of a dimensionless steam mass flux and a driving potential for the condensation process. The average heat transfer coefficient of direct contact condensation has been found to be in the range 1.0~3.5 MW/m^2-℃. Present results show that the magnitude of the average condensation heat transfer coefficient depends mainly on the steam mass flux. By using dynamic pressure measurements and visual observations, six regimes of direct contact condensation have been identified on a condensation regime map, which are chugging, transition region from chugging to condensation oscillation, condensation oscillation, bubbling condensation oscillation, stable condensation, and interfacial oscillation condensation. The regime boundaries are quite clearly distinguishable except the boundaries of bubbling condensation oscillation and interfacial oscillation condensation.

1. Introduction

Steam-water direct contact condensation phenomenon has been studied extensively, both theoretically and experimentally because of its importance in a variety of industrial operations such as underwater propulsion systems, steam jet injectors, direct contact feedwater heaters, and nuclear reactor systems (e. g., the rapid depressurization system of current PWRs and the pressure suppression system of BWRs).

There have been many experimental and theoretical works [1-19] on the direct contact condensation as summarized in Table 1. Previous studies have found that the characteristic of jet plume depends on the system operating conditions, such as the degree of subcooling of pool water, steam mass flux, nozzle

direction, and depth of submergence of the nozzle. Efforts of previous studies [1-19] to quantify these parametric effects may be broadly classified into three areas : (1) evaluation of the shape and the length of steam plume, (2) estimation of an average direct contact condensation heat transfer coefficient, (3) development of the condensation regime map.

A number of previous investigators [3,8,14,17] proposed empirical heat transfer correlations for direct condensation of vapor jets in subcooled water pool. These existing correlations were obtained by using a simplified steam-water interfacial area. These results show that the direct contact condensation heat transfer is very efficient heat transport mechanism. Sonin [4] focused his study on the turbulent intensity near the steam-water interface using a special apparatus to understand the interfacial transport mechanisms. Lim et al. [20] studied the local condensation of steam on a subcooled water layer in a cocurrent horizontal rectangular channel at atmospheric pressure : The heat transfer coefficients were found to vary from 0.0013 MW/m^2-℃ to 0.02 MW/m^2-℃, depending on whether the liquid interface was smooth or wavy, increased with increasing steam flow rates and water flow rates. Simpson and Chan [13] experimentally examined the basic mechanism of vapor jet condensation at intermediate vapor flow rate (subsonic jet) : They observed that the dynamics of subsonic jets were quite different from those of sonic jets and found that the average heat transfer for subsonic jets was about one-fifth to one-tenth of the sonic jet values. Young et al. [3] and Cumo et al. [8] investigated overall heat transport phenomena for high steam flux. Young et al. [3] proposed a Stanton-Reynolds number relation for heat transfer at the interface. Cumo et al. [8], on the other hand, suggest that the condensation heat transfer coefficient is a function of steam quality and liquid subcooling. Although they covered the overall condensation heat transfer coefficients for high steam flux region, no effort has been made to evaluate the overall heat transfer coefficient via a direct measurement of the plume surface area.

Weimer et al. [2] developed a theoretical expression for the penetration distance of vapor jets injected into a quiescent subcooled liquids of the same material : They treated the condensing jet as a two-phase, axisymmetric free jet with vapor bubbles and liquids dispersed throughout the jet. Tsai and Kazimi [18] and Chen and Faeth [19], on the other hand, presented simplified theoretical models for the penetration depth of the jet assuming an idealized plume shape and a homogeneous two-phase flow. The predicted steam plume length varies depending on the main assumptions employed. In addition, a number of experimental works with high steam mass flux have been carried out by others [3,8]. However, the existing correlations [1,2,5,15] of the steam plume length for high steam flux region do not agree with each other. Therefore, more reliable plume length correlation is desirable.

Nariai and Aya [16] developed a condensation regime map for the steam mass flux range from zero to 200 kg/m^2-sec. Cumo et al. [8] and Tin et al. [11] presented stability lines that show the boundaries between stable and unstable behavior of the vapor cones. Most of the existing condensation regime maps are based on the pool temperature and the steam mass flow rate. The rationale for using these parameters is that the steam mass flux provides a measure of the driving force exerted on the liquid side, whereas the pool temperature represents the magnitude of the thermal driving potential. It should be noted that since the previous steam condensation regime maps are limited to the value less than 200 kg/m^2-sec of the steam mass flux, the plume shapes for relatively large interfacial transport are not completely understood.

In the present work, the steam-water direct contact condensation has been experimentally investigated : A total of 346 tests (i.e., 290 tests using horizontal nozzles with four different diameters and 56 tests with two different vertical nozzles) have been conducted. As a result, correlations for an average

Table 1. Summary of Previous Studies on Direct Contact Condensation Phenomena

Author(s)	Pool P (kPa)	Pool T (℃)	d (mm)	G_o (kg/m^2-sec)	Regime Map	Plume Shape	Plume Length Correlation	Condensation Heat Transfer Rate	Remark
Kerney et al. [1]	101.3	28-79	0.4-9.5	332-2050	-	Ellipsoid	$\frac{l}{d}=0.2588\frac{(G_o/G_m)^{0.5}}{B}$	$h=1.932c_pG_m$ [1]	Horizontal
Weimer et al. [2]	4.3-38	24-38	3.17	1.17-4.13[2]	-	Homogeneous Two-Phase	$\frac{l}{d}=17.75\frac{(G_o/G_s)^{0.5}}{(\rho_\infty/\rho_s)^{0.5}B}$	-	
Young et al. [3]	101.3-380	37	6.4[3]	341-746	Six Regions	More or less Conical	-	$St=6.5Re^{-0.40}$	
Sonin [4]	101.3	40-95	5.5-10.7	300-500	-	-	-	$h=0.014\rho c_p v^{*4}$	
Standford & Webster [5]	101.3	23.9-60	10.9-52.5	54-475	-	Nearly Conical	23.9~37.8℃: $\frac{l}{d}=3.0\ln G_o-15.691$ 37.8~60.0℃: $\frac{l}{d}=3.18\ln G_o-16.6123$	-	Vertical
Kudo et al. [6]	101.3	20-50	6-27.5	120-540[5]	-	Cone	$\frac{l}{d}=\frac{1}{2a\phi_1}$	-	
Chan [7]	101.3	50-95	3.18-12.7[3]	200-400	-	Ellipsoid	-	-	
Cumo et al. [8]	101.3	20-80	1	300-2500	Stability Map	Cone	-	$h=8\times10^5\Delta T^{-0.3552}$[6]	
Arimobu [9]	101.3	20-92	16.1-27.6	5-100	Six Regions	-	-	-	
Chan and Lee [10]	101.3	40-90	51	0-175	Three Modes	-	-	-	
Tin et al. [11,12]	101.3	20-70	2-6	200-800	Stability Map	Cone	$\frac{l}{d}=\frac{1}{2a\phi_1}^{\eta}$	-	
Simpson and Chan [13]	101.3	35-75	6.35-22.2	147-333	-	-	-	~1.0MW/m^2-℃	
Fukuda [14]	101.3	25-90	8-27.6	50-400	Five Types	Ellipsoid	-	$h=43.78\frac{k_f}{d}(\frac{dG_o}{\rho\mu_f})^{0.9}\frac{c_p\Delta T}{h_{fg}}$	
Tin et al. [15]	101.3	20-75	2-6	200-750	-	Ellipsoid	$\frac{l}{d}=.5778\frac{\rho_g}{\rho_f}B^{-0.7084}Fr^{0.2101}Re^{0.6553}$	-	
Nariai and Aya [16]	101.3	20-80	18.29	0-200	Six Regions	-	-	-	
Aya and Nariai [17]	101.3	10-85	18.29	0-40	Four Regions	-	-	Chugging:2.0MW/m^2-℃ CO: 0.1~1.0MW/m^2-℃	
Tsai & Kazimi [18]	-	-	-	-	-	Ellipsoid	$1+\frac{4SB(l/d)^2}{(4l/d-1)^{1.5}}[\frac{2l}{d}\sin^{-1}(\frac{d}{2l}-1)+(\frac{d}{2l}-1)\sqrt{4l/d-1}-\pi\frac{l}{d}]=0$	-	Theoretical Approaches
Chen and Faeth [19]	-	-	-	-	-	Homogeneous Two-Phase	Model Using Locally Homogeneous Flow with k-ε-g Turbulent Model	-	

Note. [1] Derived from their experimental correlation, [2] G_o/G_s, [3] Convergent nozzle, [4] Developed using a special apparatus, [5] Steam velocity in m/sec, [6] Derived from their experimental correlation substituted by quality x=1.0, [7] Same concept as Kudo et al. [6] with a slight modification

steam-water direct contact condensation heat transfer coefficient and dimensionless steam plume lengths have been obtained. In addition, a qualitative steam-water direct contact condensation regime map for high steam mass flux region ($G>200\,kg/m^2$-sec), in particular, has been developed.

2. Descriptions of Experiment

2.1. Experimental Apparatus

The experimental apparatus is designed to allow controlled horizontal or vertical injections of steam into a pool of subcooled water with various nozzle diameters. A schematic diagram of the experimental apparatus is shown in Fig. 1. The steam is supplied by a three-phase Sussman boiler. The boiler has the maximum steam generation rate of 0.023 kg/sec with automatic pressure control and a feeding system for continuous operation. The injected steam quality is designed to be very close to 1.0, which has been con firmed by the temperature and the pressure measurements made at the downstream of the flowmeter. The steam mass flow rate is measured by a piezoelectric sensor delta flowmeter. The flow control valve is connected by a flange, where the flow path is slightly contracted from 0.0127 m to 0.01085 m in diameter. A 0.12 m long horizontal injector is submerged in the pool water of the test chamber. The nozzles for injection are made of straight double-walled pipes to prevent the occurrence of steam condensation along the inner surface of the nozzle.

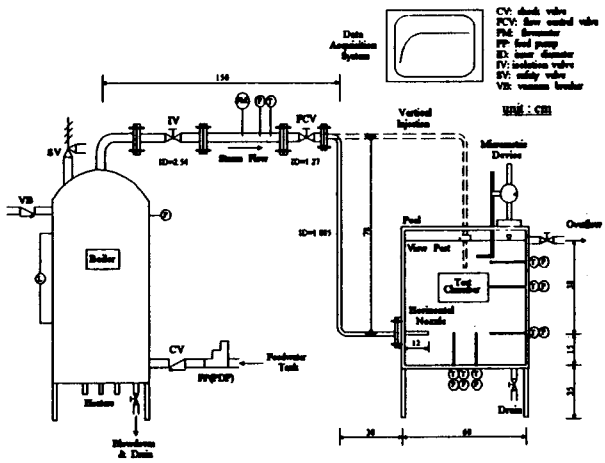

Fig. 1. Schematic Diagram of the Experimental Apparatus

The upper part of the cubic test chamber is open to the ambient with an overflow as shown in Fig. 1. A number of penetrations on the bottom and the side walls of the test chamber allow the insertion of various sensor probes. Glass windows on the back and the front walls allow high speed photography of the steam jet injection phenomenon. The dynamic pressure signals are obtained by six pressure transducers mounted on the side and bottom walls of the test chamber. The pool temperature is measured by six K-type thermocouple probes protruding through sealed penetrations on the walls. A mobile thermocouple probe, designed to measure the liquid temperature in the jet exit region, is operated manually from the outside of the test chamber during the test.

The digital sampling system consists of an eight channel analog to digital (A to D) converter and an IBM personal computer which enables the monitoring of the sampling process using a customized computer program. The maximum sample frequency of the A to D converter is 10^3 samples per second, which was found to be sufficient to investigate the phenomena of interest in this study. A digital temperature recorder, HP3467A Logging Multiplier, is used for temperature recording. An oscilloscope is used to measure the dynamic pressure wave amplitude and frequency during the test.

2.2. Test Parameters and Procedure

The test matrix used to obtain the plume shape, length and the average heat transfer coefficients is summarized in Table 2, whereas the test matrix used to develop the condensation regime map is shown in Table 3. The pool subcooling temperature ranges from 13 to 88 ℃ ; the jet exit nozzle diameters are

0.00135 m, 0.00445 m, 0.00765 m, and 0.01085 m; the nozzle orientations are horizontal and vertical (facing downward); and steam mass fluxes at the nozzle exit are in the range of 0~1500 kg/m^2-sec. For all of these tests, the ambient pressure is maintained at atmospheric, and the nozzle exit is located at 0.38 m below the free surface of the pool water for horizontal injections and 0.12 m below for vertical injections.

Prior to the injection of steam, the data acquisition system is calibrated and programmed for each experimental run. The test chamber and the boiler are filled with degassed and demineralized water. The test procedure is as follows:

① Turn on the boiler relay and the heaters.
② Open the boiler isolation valve until the boiler pressure reaches the operating pressure.
③ Preheat the system pipings by opening the flow control valve.
④ Turn on the data acquisition system.
⑤ Obtain steady flow condition by controlling the flow control valve.
⑥ Start logging experimental parameters.

Table 2. Test Matrix for the Plume Shape, Length, and the Average Heat Transfer Coefficient Evaluations

Nozzle Dia. (mm)	Pool Temp. (℃)	No. of Runs	Nozzle Orientation	Total No. of Runs
d=1.35	19~82	21	Horizontal (s=0.38m)	141
d=4.45	13~76	23		
	16~87	29		
d=7.65	22~84	16		
	24~80	13		
	28~81	14		
	16~76	14		
d=10.85	18~62	11		
d=7.65	27~81	16	Vertical (s=0.12m)	16

Table 3. Test Matrix for Condensation Regime Map Development for High Steam Mass Fluxes

Nozzle Dia. (mm)	Pool Temp. (℃)	No. of Runs	Nozzle Orientation	Total No. of Runs
d=4.45	17~83	39	Horizontal (s=0.38m)	149
d=7.65	12~82	45		
d=10.85	20~82	65		
d=10.85	16~81	40	Vertical (s=0.12m)	40

3. Experimental Results and Discussion

First, to measure the plume shape and the average heat transfer coefficient, 141 tests have been conducted using four different diameter horizontal nozzles. In addition, 16 tests have been performed with a vertical injection nozzle to compare with the result of horizontal injections as summarized in Table 2. Reproducibility tests have been carried out with a 0.00445 m diameter nozzle (repeating the same test twice) and also with 0.00765 m diameter nozzle (repeated four times under the same test conditions). Also, to develop a condensation regime map including high steam mass flow rate (i.e. $G>200$ kg/m^2-sec), in particular, a total of 189 tests have been conducted using horizontal and vertical nozzles as summarized in Table 3.

3.1. Plume Length and Shape Measurements

To measure the size of steam plume, enlarged photographic images are traced on a graph paper using a slide projector. Axial and radial positions of the plume contour are scaled to actual values from the reference scale, that is, the injector outer diameter. The steam plume surface area measurement is very important to calculate the average direct contact condensation heat transfer coefficient.

It has been found that there is a two-phase mixture region around the steam vapor cone near the end point of the plume. In this work, the two-phase mixture region has not been included in the plume length. The plume shape has been idealized as an ellipsoid when the end point of the plume is not clear. This is the main reason why the plume shapes pres-

ented by previous authors for high steam mass flux are different from each other and there are considerable differences among the previous work by others [1-3,5-8,12,14,15,18,19]. When the saturated steam is injected into a stagnant pool, in the present work, basically three different shapes of steam plume (i.e., conical, ellipsoidal, and divergent shape) have been generated as shown in Figs. 2 and 3.

For the case of large subcooling and low steam mass velocity, the plume shape becomes nearly conical shape as shown in Fig. 3(a). For a relatively large nozzle diameter the plume shape tends to become conical. For large and intermediate subcooling, the plume shape becomes ellipsoidal as shown in Fig. 3 (b). All of the ellipsoidal shape plumes show that there is an external expansion region adjacent to the nozzle exit, which has also been observed by Weimer et al. [2]. The plume has a slight necking or gradient change, that is, a transition point at the steam-water interface, which has also been found by Tin et al. [15]. The conical and ellipsoidal shapes are observed in the stable condensation (SC) region of the condensation regime map (as will be shown in Fig. 10). As the subcooling decreases, the transition point disappears and the plume shape becomes an oval. When the subcooling is small, the plume shape becomes divergent for wide range of steam mass velocities as shown in Fig. 3(c). This is the typical shape found in the interfacial oscillation condensation (IOC) region of the condensation regime map. The plume surface oscillates radially and the end point of the plume oscillates back and forth.

In general, the plume shape has a short divergent tract for high steam mass flux and its diameter increases as the pool temperature increases as observed by Tin et al. [15]. The steam plume behavior is found to be consistent with the theoretical understanding of Tsai and Kazimi [18] and Chen and Faeth [19]. The experimental data show that the ratio of the maximum plume diameter to the injector inner diameter ranges from 1.0 to 2.3. In the region immediately following an external expansion near the

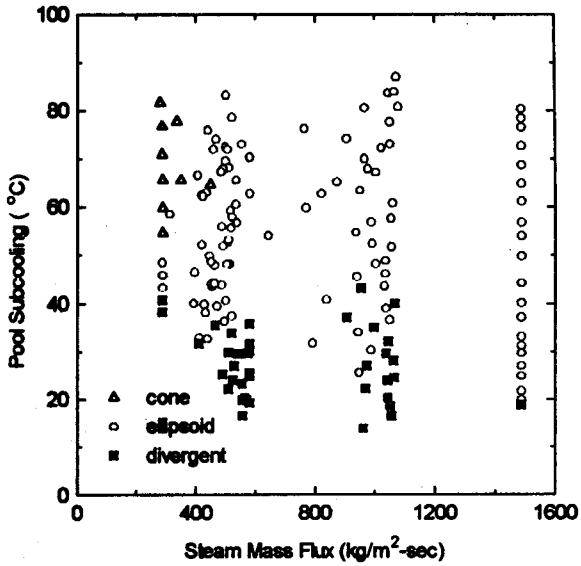

Fig. 2. Plume Shape Distribution (Nozzle Inner Diameter d=1.35-10.85mm)

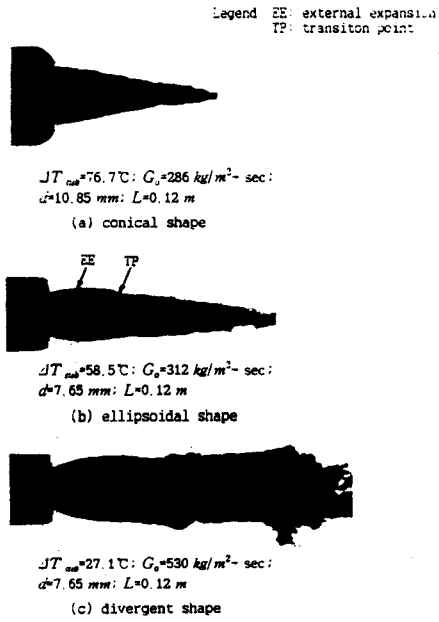

Fig. 3. Steam Pluem Shapes Observed with Horizontal Nozzles Under Different Experimental Conditions

vicinity of the transition point, liquid entrainment may be occurring at the inner surface of the plume

as predicted by van Rossum [21] and Mandhane et al. [22] and measured by Tin et al. [15]. Near the end region, where the plume shape terminates, the flow is observed to be two-phase due to steam entrapment by the liquid region as assumed by Weimer et al. [2] and Chen and Faeth [19].

Major parameters for plume length estimation used by previous workers [1,2,5,6,12,15,18,19] include the steam mass velocity, condensation driving potential (B), the transport modulus or modified Stanton number using steam mass velocity (S), and relative density difference between steam and water. A theoretical relation between dimensionless plume length and other parameters for ellipsoidal steam plume can be derived as follows [1]:

Assuming an axially symmetric flow and employing the coordinate system illustrated in Fig. 4, the conservation of vapor mass requires

$$\frac{d\dot{m}}{dx} = -2\pi r M \tag{1}$$

where the rate of condensation per unit surface area (M), can be obtained from the following interfacial heat transfer relation

$$h_{fg} M = h(T_s - T_l) \tag{2}$$

The vapor mass flow rate($\dot{m}$) can be related to the mass velocity (G) by

$$\dot{m} = \pi r^2 G \tag{3}$$

Substituting Eqs. (2) and (3) into Eq. (1) yields

$$\frac{d\sqrt{\dot{m}}}{dx} = -\sqrt{\pi G} \cdot SB \tag{4}$$

where the transport modulus (S) and the condensation driving potential (B) are defined as:

$$S = \frac{h}{c_p G} \tag{5}$$

$$B = \frac{c_p(T_s - T_l)}{h_{fg}} \tag{6}$$

The boundary conditions for Eq. (4) are

$$x = 0, \quad \dot{m} = \dot{m}_o; \quad x = l, \quad \dot{m} = 0 \tag{7}$$

Assuming that an appropriate mean value over the plume can be chosen for G and S, Eq. (4) can be integrated to yield the dimensionless plume length as:

$$\frac{l}{d} = 0.5\sqrt{\frac{G_o}{G_m}}/(S_m B) \tag{8}$$

Equation (8) shows that the dimensionless plume length depends on the ratio of the steam mass flux at the nozzle exit and the mean value of the plume ($\frac{G_o}{G_m}$), the condensation driving potential (B), and the mean transport modulus (S_m). It should be noted that G_m has been chosen to be equal to the critical vapor mass velocity at the ambient pressure of the present tests, i.e., 275 kg/m^2-sec.

In general, the dimensionless plume length can be expressed as:

$$\frac{l}{d} = f(B, \frac{G_o}{G_m}, S_m) \tag{9}$$

Unfortunately, the mean value of the transport modulus (S_m) is not a directly measurable quantity. Therefore, an empirical correlation for the plume length without S_m has been derived by fitting the plume length data as:

$$\frac{l}{d} = 0.5923 B^{-0.66} (\frac{G_o}{G_m})^{0.3444} \tag{10}$$

The dimensionless plume length given by Eq. (10) is plotted with the plume length data in Fig. 5. Most of the experimental data are within the band of ± 20%. In the region where the dimensionless plume

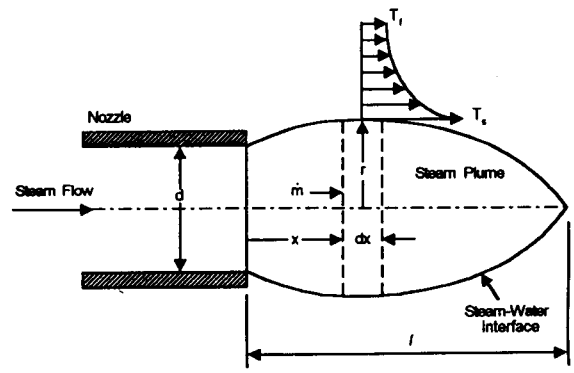

Fig. 4. Schematic of the Condensing Plume

length is less than 5, the predicted values underestimate the experimental data. Conversely, in the region where the dimensionless plume length is greater than 5, the predicted values overestimate the data. For a given value of steam mass flux, the dimensionless plume lengths obtained by the previous and the present correlations are shown in Fig. 6. As shown in Fig. 6, most of the previous correlations overestimate the plume length. It should be noted that as the liquid pool temperature increases, the disagreement between the plume length correlations and the present experimental data becomes significant, which is mainly due to the assumption of the ellipsoidal plume and the increased uncertainty in determining the length of unstable plumes.

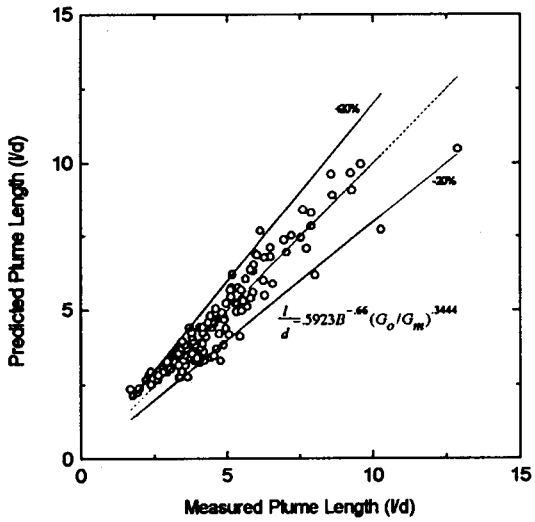

Fig. 5. Comparison between Measured and Predicted Dimensionless Plume Lengths

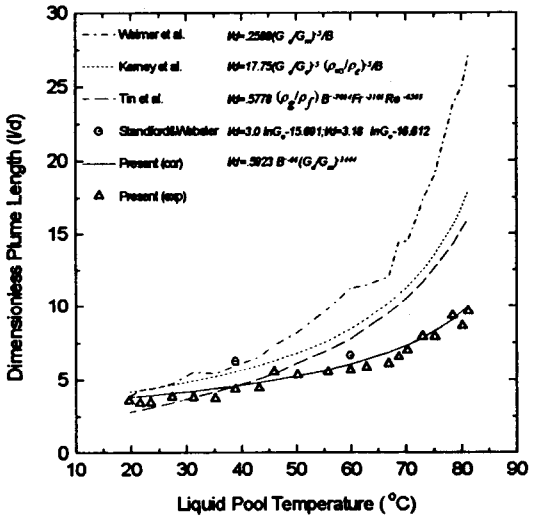

Fig. 6. Comparison of Plume Lengths Predicted by Various Correlations with Present Experimental Data (d=1.35mm, G_o=1488kg/m^2-sec)

3.2. Average Condensation Heat Transfer Coefficient Evaluation

The average heat transfer rate (Q) of the direct contact condensation can be expressed as :

$$Q = hA(T_s - T_f) \quad (11)$$

where A, T_s and T_f are the plume surface area, the saturation temperature, and the liquid pool temperature, respectively. Using the measured heat transfer area, the average heat transfer coefficients are evaluated and the results are plotted in Fig. 7. As can be seen in this figure, the average heat transfer coefficient varies from 1.0 to 3.8 MW/m^2-℃, which is

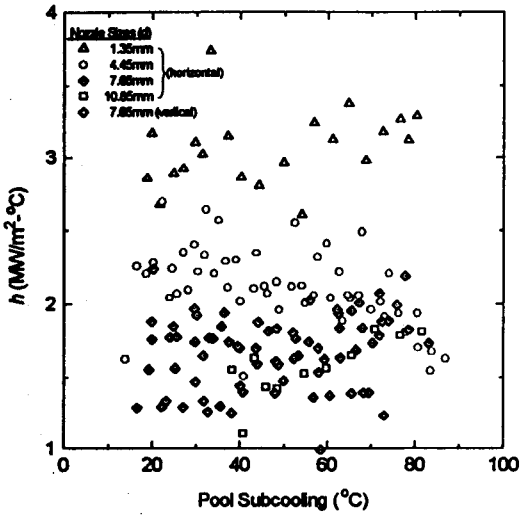

Fig. 7. Average Steam-water Direct Contact Condensation Heat Transfer Coefficient for High Steam Mass Fluxes as a Function of Pool Subcooling for Various Nozzle Diameters

comparable to those obtained by previous workers [1,3,8].

In a system where the steam and the water coexist, the condensation heat transport is mainly controlled by the water side [20]. When steam is injected into a stagnant pool of water, however, the steam velocity is very large. Therefore, its momentum and energy are transported instantly to liquid side through the interface. According to the Kudo's analytical prediction [6], the interfacial velocity is as high as 26 m/sec when the steam velocity is 400 m/sec. If one uses the interfacial velocity as the turbulent intensity for the correlation developed by Sonin [4], the heat transfer coefficient is obtained as 1. 5 MW/m^2·℃.

As shown in Fig. 7, the pool subcooling is not important for the average heat transfer coefficient. It is interesting to note that the necking heat transfer coefficient obtained by Simpson and Chan [13] is not a strong function of the pool subcooling either. Instead, the size of the injection nozzle has been found to be important. The horizontal injection data clearly shows that the average heat transfer coefficient increases significantly as the nozzle diameter is reduced. In other words, the direct condensation heat transfer occurs more efficiently when the steam is injected through smaller diameter nozzles.

To correlate the experimental data, one can use Eq. (9) in a slightly different form as :

$$S_m = f(B, \frac{l}{d}, \frac{G_o}{G_m}) \tag{12}$$

Using the least square method to fit the experimental data, following expression for the average heat transfer coefficient has been found :

$$h = 0.8012 c_p G_m B^{\,0.6247} (\frac{l}{d})^{\,1.0079} (\frac{G_o}{G_m})^{0.7185} \tag{13}$$

When the measured average heat transfer coefficient data are plotted against the predicted values obtained by Eq. (13), the agreement is within ±15% for most of the experimental data as can be seen in Fig. 8.

In general, the dimensionless plume length in Eq.

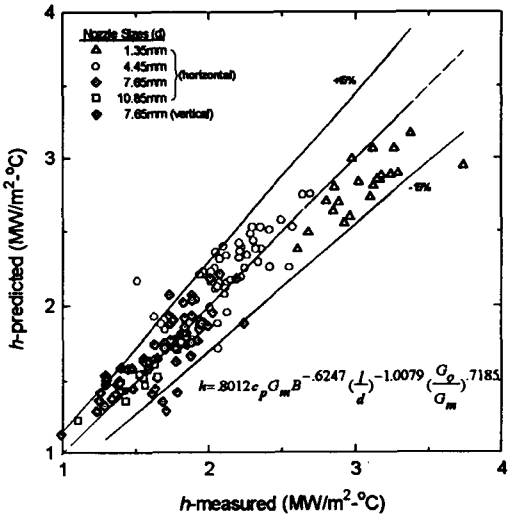

Fig. 8. Comparison between Measured and Predicted Average Steam-water Direct Contact Condensation Heat Transfer Coefficient

(13) is not known. One can obtain the more useful heat transfer correlation by inserting Eq. (10) into Eq. (13) as :

$$h = 1.3583 c_p G_m B^{0.0405} (\frac{G_o}{G_m})^{0.3714} \tag{14}$$

Figure 9 shows the comparison of average heat transfer coefficient between the data and predicted values obtained by Eq. (14). This figure shows that most of the experimental data agree with Eq. (14) within ±30%. According to Eq. (14), the average condensation rate or heat transfer coefficient for steam injection into a stagnant pool of water increases with increasing steam flow rate and the degree of subcooling, which is in agreement with the results reported by Lim et al. [20]. However, the effect of liquid subcooling on the average heat transfer coefficient is found to be much smaller than that of the steam flow rate. Even though the exponents for c_p and G_m are relatively large, the effects of these parameters on the average heat transfer rate are insignificant since the variations of these values are very small under typical operating temperature conditions. Therefore, one can conclude that the major controlling parameter in the direct contact condensation energy

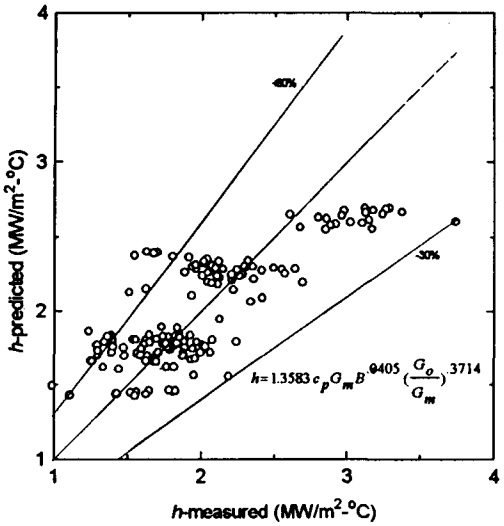

Fig. 9. Comparison Between Measured and Predicted Average Steam-water Direct Contact Condensation Heat Transfer Coefficient

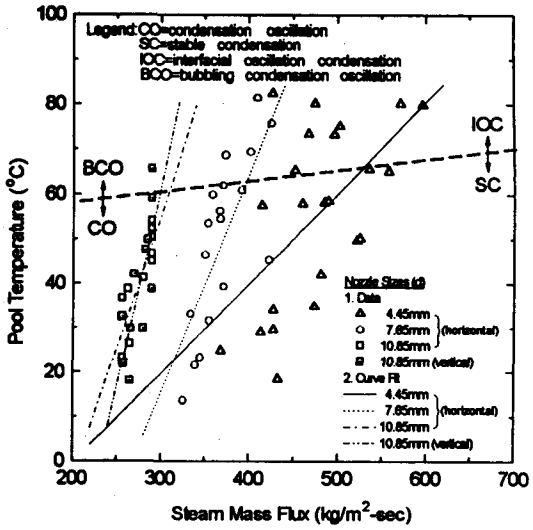

Fig. 10. Typical Direct Condensation Regime Map for Various Nozzle Inner Diameter(d=4.45−10.85mm) and Nozzle Length(L=0.12m)

transport is the steam mass flow rate. If the steam conditions, that is, the subcooling temperature and the steam mass flux at the injector exit, are known, the average condensation heat transfer rate through the liquid-vapor interface can be estimated by Eq. (14).

3.3. Condensation Regime Map for High Steam Flux

The pool water temperature (or liquid subcooling) represents the magnitude of thermal driving force between the steam plume and the bulk liquid region. The energy transferred from steam to the liquid interface can be transported to the bulk liquid region by the turbulent motion which originates at the vapor-liquid interface. Based on these considerations, the steam mass velocity and the pool water temperature are used as the major parameters for the condensation regime map in a manner similar to the methods used by previous workers [8-11,14,16,17].

In the present work, six regimes of direct contact condensation have been identified by visual and acoustical methods that use oscilloscope outputs from dynamic pressure transducers. In Fig. 10, however, only four regimes of direct contact condensation that occur at particularly high steam mass flux ($G>200\,kg/m^2$-sec) are shown. That is, the 'chugging' (C) and 'transition region from chugging to condensation oscillation' (TC) regions that occur at lower steam mass flux ($G<200\,kg/m^2$-sec) are not shown for brevity. The 'chugging' (C) (i.e., periodic build-up and collapse of steam plumes) occurs at low liquid temperature and low steam velocity. In this region, as the steam plume collapses, the subcooled water rushes into the nozzle due to the negative pressure generated by a sudden condensation. The water is then slowly pushed out by the steam again. During the 'chugging', the amplitude of the pressure oscillation measured at the test chamber wall, is relatively large and irregular.

As the steam mass flux is increased, a 'transition region from chugging to condensation oscillation' (TC) is found to occur where the frequency of the pressure oscillation is between 20 Hz and 80 Hz. In this region, the subcooled water does not enter the nozzle any more. Instead, a cloud of tiny steam bubbles is formed near the nozzle exit, which is the pre-

cursor of the stable steam plume.

Further increase of the steam mass flux results in the 'condensation oscillation' (CO) as identified by previous works [9,14,16,17]. The frequency of the 'condensation oscillation' is quite high (i.e. greater than 100 Hz). Steam condenses outside the nozzle and the steam-water interface oscillates violently and the ambient water moves back and forth according to the plume motion.

The 'bubbling condensation oscillation' (BCO) occurs within the same steam mass velocity region of the 'condensation oscillation' but at higher liquid temperature. The steam plumes of this region are detached from injector and relatively large steam bubbles of irregular shape are condensed and/or rise to the free surface.

When the steam mass flux is relatively large, a 'stable condensation' (SC) occurs. The 'stable condensation' can be characterized as a quiet condensation. As the pool water temperature increases, the interface of steam plume becomes unstable. This region is called as an 'interfacial oscillation condensation' (IOC). On the boundary between SC and IOC, the frequency of the detected pressure wave signals is reduced for higher pool temperature. Moreover, the amplitude of the pressure wave is increased as the pool temperature is increased. In Fig. 10, the BCO and IOC regions are represented by a dotted line as the transition characteristics can not be identified distinctly by acoustic and pressure pulse measurements. It has been found that the boundaries between regions vary for different injector nozzle size and as the nozzle size decreases these boundaries shift slightly to higher steam flux region. The 'condensation oscillation' region becomes wider as the pool water temperature increases. This means that as the pool water temperature is raised (or subcooling is decreased) the steam mass flux should also be increased to maintain the 'stable condensation'. This is in agreement with the results of Cumo et al. [8] and Tin et al. [11]. It should also be noted that the required steam mass flux for a 'stable condensation' increases as the injector nozzle diameter decreases. This injector size dependancy agrees with that found by Tin *et al.* [11].

4. Conclusions

Three plume shapes, that is, conical, ellipsoidal, and divergent shape that depend on the steam mass flux and the liquid subcooling, have been found. In general, the conical and the ellipsoidal shapes are observed at high liquid subcooling while the divergent shape is observed at low liquid subcooling. The expansion ratio of the maximum plume diameter to the injector inner diameter ranges from 1.0 to 2.3. An empirical correlation is proposed to predict the steam plume length as a function of a dimensionless steam mass flux and a driving potential for the condensation process (B).

The average heat transfer coefficient of direct contact condensation for high steam mass velocities is found to be in the range of 1.0~3.5 MW/m^2-℃. An empirical correlation is also proposed to predict the average heat transfer coefficients. The average condensation heat transfer coefficients increase with increasing steam mass flux and is slightly influenced by the degree of subcooling. It is also found that the direct contact condensation heat transfer is more efficient when smaller diameter nozzles are used.

Various direct contact condensation regimes have been identified as shown in the direct condensation regime map: They are chugging (C), transition region from chugging to condensation oscillation (TC), condensation oscillation (CO), bubbling condensation oscillation (BCO), stable condensation (SC), and interfacial oscillation condensation (IOC). It is found that the frequency and the amplitude of the pressure pulse generated by the steam jet can be used to characterize each condensation regime. Particularly, the amplitude of the pressure pulse is highest for the chugging regime and the frequency for the condensation oscillation regime is greater than 100 Hz.

Nomenclature

A plume surface area, m^2

B driving potential for condensation, $\frac{c_p(T_s-T_f)}{h_{fg}}$

c_p liquid specific heat, J/kg-℃

d injector inner diameter, m

G steam mass flux, kg/m^2-sec

h heat transfer coefficient, W/m^2-℃

h_{fg} latent heat of vaporization, J/kg

l steam plume length, m

$\dot{m}$ steam flow rate, kg/sec

M rate of condensation per unit area, kg/m^2-sec

Q total heat transfer rate, W

r radius of steam plume at axial position x, m

s submerged depth of the injector, m

S dimensionless transport modulus or modified Stanton number, $\frac{h}{c_pG}$

T temperature, ℃

x axial position from nozzle exit, m, or steam vapor quality

Subscripts

e external expansion condition

f liquid phase

m mean value for steam plume

o injector exit condition

s saturation

References

1. P.J. Kerney et al., "Penetration Characteristics of a Submerged Steam Jet," AIChE J., Vol. 18, No. 3, pp. 548-553, (1972)
2. J.C. Weimer et al., "Penetration of Vapor Jets Submerged in Subcooled Liquids," AIChE J., Vol. 19, No. 3, pp. 552-558, (1973)
3. R.J. Young et al., "Vapor-Liquid Interaction in a High Velocity Vapor Jet Condensing in a Coaxial Water Flow," Proc. 5th Int. Heat Transfer Conf., Tokyo, Vol. 3, pp. 226-230, (1974)
4. A.A. Sonin, Suppression Pool Dynamics Research at MIT, NUREG/CP-0048, pp. 400-421, (1984)
5. L. E. Stanford and C.C. Webster, Energy Suppression and Fission Product Transport in Pressure-Suppression Pools, ORNL-TM-3448, (1972)
6. A. Kudo et al., "Basic Study on Vapor Suppression," Proc. 5th Int. Heat Transfer Conf., Tokyo, Vol. 3, pp. 221-225, (1974)
7. C.K. Chan, "Dynamical Pressure Pulse in Steam Jet Condensation," Proc. 6th Int. Heat Transfer Conf. Toronto, Vol. 5, pp. 395-399, (1978)
8. M. Cumo et al., "Heat Transfer in Condensing Jets of Steam in Water," Proc. 6th Int. Heat Transfer Conf. Toronto, Vol. 5, pp. 101-106, (1978)
9. M. Arinobu, "Studies on the Dynamic Phenomena Caused by Steam condensation in Water," Proc. of ANS-ASME-NRC Int. Topical Meeting on Nuclear Reactor Thermal Hydraulics, vol. 1, Saratoga Springs, New York, pp. 293-302, (1980)
10. C.K. Chan and C.K. B. Lee, "A Regime Map for Direct Contact Condensation," Int. J. Multiphase Flow, Vol. 8, No. 1, pp. 11-20, (1982)
11. G. D. Tin et al., "Pressure and Temperature Measurement in a Vapor Condensing Jet," Proc. 7th Int. Heat Transfer Conf., Muchen, Vol. 6, pp. 159-164, (1982)
12. G.D. Tin et al., "Experimental Study on Steam Jet Condensation in Subcooled Water Pool," Proc. 3rd Multi-Phase Flow and Heat Transfer Symp. Workshop, Miami Beach, Florida, U.S.A., pp. 815-830, (1983)
13. M.E. Simpson and C.K. Chan, "Hydrodynamics of a Subsonic Vapor Jet in Subcooled Liquid," J. of Heat Transfer, Vol. 104, pp. 271-278, (1982)
14. S. Fukuda, "Pressure Variations due to Vapor Condensation in Liquid, (II) Phenomena at Large Vapor Mass Flow Flux," J. of JNS (in Japanese), Vol. 24, No. 6, pp. 466-474, (1982)

15. G.D. Tin et al., "Thermal and Fluid-Dynamic Features of Vapor Condensing Jets," Heat and Technology, Vol. 1, No. 1, pp. 13-35, (1983)
16. H. Nariai and I. Aya, "Fluid and Pressure Oscillations Occurring at Direct Contact Condensation of Steam Flow with Cold Water," Nuclear Engineering and Design, Vol. 95, pp. 35-45, (1986)
17. I. Aya and H. Nariai, "Evaluation of Heat-Transfer Coefficient at Direct-Contact Condensation of Cold Water and Steam," Nuclear Engineering and Design, Vol. 131, pp. 17-24, (1991)
18. S.S. Tsai and M.S. Kazimi, "The Potential for Penetration of a Hot Vapor Jet into a Subcooled Liquid," ASME 76-WA/HT-78, (1976)
19. L.D. Chen and G.M. Faeth, "Condensation of Submerged Vapor Jets in Subcooled Liquids," J. of Heat Transfer, Vol. 104, pp. 774-780, (1982)
20. I.S. Lim et al., "Condensation Measurement of Horizontal Concurrent Steam/Water Flow," J. of Heat Transfer, Vol. 106, pp. 425-432, (1984)
21. J.J. van Rossum, "Experimental Investigation of Horizontal Liquid Film: Wave Formation, Atomization, Film Thickness," Chemical Engineering Science, Vol. 11, pp. 35-52, (1959)
22. J.M. Mandhane et al., "A Flow Pattern Map for Gas-Liquid Flow in Horizontal Pipes," Int. J. Multiphase Flow, Vol. 1, pp. 537-553, (1974)